Fuel Processing Technology 176 (2018) 91–100

Contents lists available at ScienceDirect

Fuel Processing Technology

journal homepage: www.elsevier.com/locate/fuproc

Research article

The effect of water addition on the surface energy, bulk and flow properties of lignite

Yong Jin, Hai-Feng Lu*, Xiao-Lei Guo, Xin Gong*

Key Laboratory of Coal Gasification and Energy Chemical Engineering of Ministry of Education, East China University of Science and Technology, Shanghai 200237, PR China

Shanghai Engineering Research Center of Coal Gasification, East China University of Science and Technology, Shanghai 200237, PR China

ARTICLE INFO

Keywords:
Surface energy
Flow properties
Bulk properties
Water addition
Model analysis

ABSTRACT

In this paper, the relationship between angle of repose, surface energy and bulk and shear properties of different particle size distribution lignite pulverized coal with different moisture content was experimentally investigated. The dry sample and wet sample were prepared under relative humidity 0% and 90%. The interactions between coal samples and polar or non-polar gaseous probes were investigated by the surface energy test with an inverse gas chromatography (IGC) technique. The compressibility test and shear test were taken by the FT4 Powder Rheometer. The changes in bulk and flow properties of different particle size distribution samples were collected as a function of water content. The results show that water content plays a significant role on the packing and flow behaviors and surface energy of the dry and wet different particle size lignite pulverized coal. The IGC tests results showed that for the relative humidity 90% samples, the water was the interior water, which played a role of improving the flowability. In the end, a model was proposed to study the relationship between angle of repose and surface energy and flowability. The model could easily predict the relationship between angle of repose with wet and dry particles. This research will provide a better understanding on how water content affects surface characteristic and the flow properties of lignite particles and will benefit to optimize the relevant unit operations.

1. Introduction

Entrained-flow pressurized gasification process, including the storage, discharge and pneumatic conveying of pulverized coals, is one of the best contemporary carbon gasification technologies [1,2]. There are various gasification materials, involving in coal, biomass, pet coke and etc. [3] Because of limitation of the energy structure and the storage of coal, lignite coal is the most widely used in the entrained-flow pressurized gasification process [3–5]. During the entrained-flow pulverized coal gasification process, moisture content of the coal is usually controlled below 2 wt% for the smooth and reliable feeding system, which needs huge amount of heating resources [6]. If the moisture content of lignite pulverized coal, rich in water, is reduced to a smaller level where the flowability will not be influenced greatly, it will make significant potential economic benefits [7]. Therefore, the study of water addition on the lignite coal is very important.

The reliable handling of wet particles is a requisite for a successful industrial application, but it still represents a scientific and technological challenge. The handling and processing of wet powders require a good understanding of their bulk mechanical behavior such as cohesiveness, flowability and aggregation [8–10]. For the particulate material, many bulk mechanical properties are related to inter-particle forces, such as van der Waals, capillary and electrostatics forces. Suitable powder conditioning may minimize the influence of capillary and electrostatic forces. However, without altering the powder composition and particle size distribution, it is not possible to change the effect of van der Waals forces in dry powders. Van der Waals force depends on the material surface free energy [11–13].

In this paper, the methodology of shear test, angle of repose test, compressibility test and surface energy test are taken to analysis the influence of moisture content on different particle size distribution. The surface energy of particles is the analogue of surface tension of liquids and determines several chemical and physical properties of materials. For example, a high surface energy means a more reactive surface [14,15]. Surface energy has also important implications in interfacial interaction processes, such as wetting, coating, mixing, compaction, cohesion and adhesion [16–18]. The surface energy determines the interactions between particles themselves as well as with other surfaces [19]. These properties require a better understanding on particles, which have not been well understood. Measurements of surface energy

* Corresponding authors.
E-mail addresses: luhf@ecust.edu.cn (H.-F. Lu), gongxin@ecust.edu.cn (X. Gong).

https://doi.org/10.1016/j.fuproc.2018.02.024
Received 13 November 2017; Received in revised form 10 January 2018; Accepted 26 February 2018

Nomenclature

AN	acceptor number
AOR	angle of repose
BET	Brunauer, Emmett and Teller
C	cohesive strength
d	particle size
d_e	equivalent mean particle size
d_s	mean surface diameter of the particles
DN	donor number
F_{ad}	inter-particle force
g	gravity
$\triangle G$	free energy
$\triangle G^d$	adsorption free energy
ΔG^{sp}	specific free energy
K	model parameter
$k_{1,2,3,4}$	coefficient of proportionality
K_A	Gutmann acid numbers
K_D	Gutmann base numbers
n	the spread of particle sizes
n/n_m	surface converge
N_A	the number of Avogadro
n_c	contacts per unit fracture area
n_{cp}	the number of micro scopic interparticle contacts per unit fracture surface area
n_{pp}	the number of macroscopic interparticle contacts per unit fracture surface area
m_1	model parameter
M_t	moisture content
R	the gas constant
$R(d)$	particle size distribution function
T	the temperature of measurement (K)
p	model parameter
V_N	the retention volume
a	the cross sectional area of the probe
γ	surface energy
γ^D	dispersive surface energy
γ_l^d	liquid dispersive surface energy
γ_s^d	solid dispersive surface energy
ρ_p	true density
$\rho_{b,0}$	bulk density
φ	the bed compactness
φ_i	angle of internal friction

of particles involve determination of long and short-range intermolecular forces, which are commonly described as London dispersive and acid/base interactions respectively [20]. Unlike flat surfaces of materials, such as the biomass particles, whose surface energy can be easily determined by contact angle measurements, the powder materials are hard to perform such measurements [21]. In this research, we used a Surface Energy Analyzer (SEA) to determine the surface energy of the lignite. Many people have studied the influence of particle size distribution and moisture content on the particle system from the stand point of flowability [22–27] and surface energy [28–31]. Sometimes the addition of moisture content is carried out by the change of relative humidity. And many researchers also studied the effect of humidity on powders [32–39]. They have concluded that with the increase of moisture content, the flowability of the particle system would be poorer [6]. Among these studies, the study of the addition of moisture content in the lignite pulverized coal by the humidity, like our system, there are few studies. Through our study, the addition of this kind of moisture content will improve the flowability. The flowability of the particle system is influenced by the particle contacts. The particle contacts can be determined by the Rumpf equation or the modified Rumpf equations to study the relationship between tensile strength and interparticle forces [32–34]. This method can provide people a quantitative description of the relative strength among particles.

To better guide the industrial process, this study also investigates the relationship between particle-scale interactions dominated by the cohesive van der Waals force and powder flow performance. For the experiment materials, the surface energy was determined from the particle scale. The compressibility test and angle of repose test was carried out from the bulk scale. In the last part of the paper, the relationship between the bulk and surface properties was established by using a model to predict the angle of repose. These results will be helpful to gain process control on unit operation such as storage, discharge and pneumatic conveying.

2. Materials and methods

2.1. Materials

The lignite pulverized coal was obtained from Yangzi Petrochemical Company limited in China and used without any modifications. The raw sample was sieved by air classifier (Retsch AS200 Jet Air). The particle size distribution of the particles was measured with a particle size analyzer (Malvern Mastersizer 2000MU) (Fig. 1). The particle size

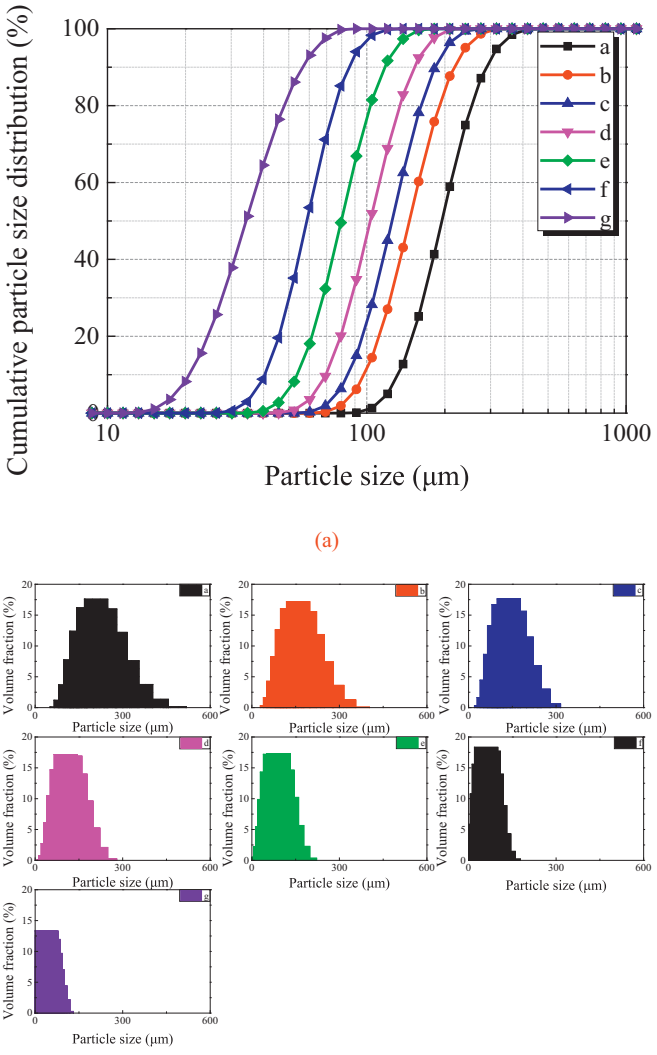

Fig. 1. The Mastersizer 2000 particle size distribution for the lignite pulverized coal particle. (a) cumulative particle size distribution; (b) histograms of particle size distribution.

Table 1
Characteristic diameters of the particle size distribution and the fitting value of parameter *n*.

Material	d_v(μm)	d_s(μm)	*n*
a	234.02	214.32	4.92
b	175.24	159.90	4.54
c	149.57	137.29	4.91
d	123.56	113.04	5.23
e	95.40	87.50	4.49
f	70.13	64.72	4.87
g	42.08	36.55	3.73

distribution can be described by the Rosin–Rammler equation:

$$R(d) = 100 - \varphi = 100\exp\left[-\left(\frac{d}{d_e}\right)^n\right] \quad (1)$$

where R(d) is the particle size distribution function; d is the particle size; d_e is the equivalent mean particle size; and n is a parameter which describes the spread of particle size distribution. If the value of n is large, the range of particle sizes distribution will be narrow.

Fig. 1 shows the measured particle size distribution characterized as cumulative particle size and histograms of particle size distribution. Table 1 presents the characteristic diameters of the measured particle size distribution and the fitting parameter n from Eq. (1).

True density ρ_p of the lignite pulverized coal particle was measured with an Accupyc 1330 pycnometer (Micromeritics Instrument Corporation, USA) and the Brunauer, Emmett and Teller (BET) specific surface area of tested particles was determined from octane sorption isotherm using IGC-SEA (Inverse Gas Chromatography-Surface Measurement Systems Ltd, UK).

Table 2
Physical properties of dry lignite pulverized coal particle.

Material	BET($m^2 \cdot g^{-1}$)	ρ_p($kg \cdot m^{-3}$)
Lignite	4.22	1460

The seven samples were dried first to remove total moisture and the surface energy test and flowability test were carried out for the dry particle. The test environment was kept at 25 °C and kept the sample dry during the whole experiment. For preparation of the wet samples, the dry samples were put in the constant temperature and humidity incubator (Binder KMF115) at the atmosphere of relative humidity 90% under 25 °C. The moisture content (M_c) was determined by infrared moisture meter (Sartorius MA150), seen in Supporting information (Table S1). Obviously, the moisture content was nearly the same.

2.2. Surface energy analysis

The chromatographic measurements were performed with an IGC Surface Measurement System (SMS) Ltd gas chromatograph (London, United Kingdom) equipped with a thermal conductivity detector (TCD) and a flame-ionization detector (FID). Chromatographic column was a hollow glass tube, I.D. 3 mm, length 30 cm. The column temperature was set as 105 °C, whereas the detector and injector were heated at 180 °C. Helium was used as carrier gas. Flow-rate of 15 $ml \cdot min^{-1}$ was selected. Relative humidity of carrier gas was equal to 0 and 90% for the dry and wet test. The humidity was controlled automatically because the IGC equipment used in this paper could give the possibility for precise humidity regulation and therefore allows to study properties at well-defined conditions. Measurements were carried out at infinite dilution. The solvents were used as test compounds during IGC experiments (seen in Supporting information Table S2). The sample column was run at a surface coverage of 0.01 with non-polar probe molecules (hexane, heptane, octane, and nonane) on the materials to determine the dispersive surface energy. Parameters describing surface properties (γ_s^d, K_A and K_D) were determined using physicochemical parameters of test compounds summarized in Table S2. The retention time obtained from methane injection was used as the retention time of the non-adsorbing probe. The data were analyzed with the advanced Cirrus Plus SEA Data Analysis Software (version 1.2.1.2).

2.3. Angle of repose test

Angle of repose (AOR) is one of the key factors in characterizing the flow behavior of powders, which is the steepest angle of descent of a granular material or dip relative to the horizontal plane in which a material could be piled without slumping. A Hosokawa Powder Tester model PT-X was used to measure the angle of repose (AOR). The procedure follows ASTM D6393-99 standard “Bulk Solids Characterization by Carr Indices”. The experiment was carried out three times. During the procedure of AOR measurement, the powder was placed in the powder holder of the device. The equipment was set to run for 180 s. After 180 s's running time, the AOR was recorded by the equipment. The AOR is also affected by the addition of solvents. If a small amount of water fills the gaps between particles, the angle of repose increases due to electrostatic attraction of water on the mineral surfaces.

2.4. Bulk and shear properties test

The compressibility of the materials was characterized by FT4 powder Rheometer (Freeman technology, UK) using compressibility module. Details of measurement principle and operation of FT4 are available in the reference [11]. Briefly, in the compressibility module, a volume of 85 ml powders was loaded in the testing vessel. Before each test, the sample was first prepared by powder conditioning. Splitting vessel removed any residual materials to build a uniform and loose conditions for the bed of powders. Then, a vented piston was used to compress the powders with stepped normal stresses of 1, 2, 4, 6, 8, 10, 12 and 15 kPa. The distance traveled by the piston was measured for each applied normal stress. The bulk density was calculated from the volume below the piston. The shear test under 3 kPa, 6 kPa and 9 kPa are also carried out by FT4. To eliminate the time consolidation effect, the blade stirred in the vessel for creating loose conditions where the torque is zero.

3. Results and discussions

3.1. Surface properties

3.1.1. Surface energy determination

Fowkes [40] suggested that the surface energy could be divided into two parts, such as the dispersive part and the specific part.

$$\gamma = \gamma^d + \gamma^{sp} \quad (2)$$

Therefore, the free energy change is the combination of polar and non-polar interactions depending of the nature of the injected probes.

$$\Delta G = \Delta G^d + \Delta G^{sp} \quad (3)$$

The free surface energy was determined by some n-alkenes, which had dispersive forces on the solid phase. So the dispersive free surface is

$$\Delta G = \Delta G^d = RT \ln V_N + \text{Constant} \quad (4)$$

where R is the gas constant, 8.314 ($J \cdot mol^{-1} \cdot K^{-1}$), T is the test temperature (K), V_N is the retention volume (m^3), and Constant depends on the reference state. The free energy changes of adsorption can be expressed as:

$$\Delta G = -2V_N a\sqrt{\gamma_s^d \gamma_l^d} \quad (5)$$

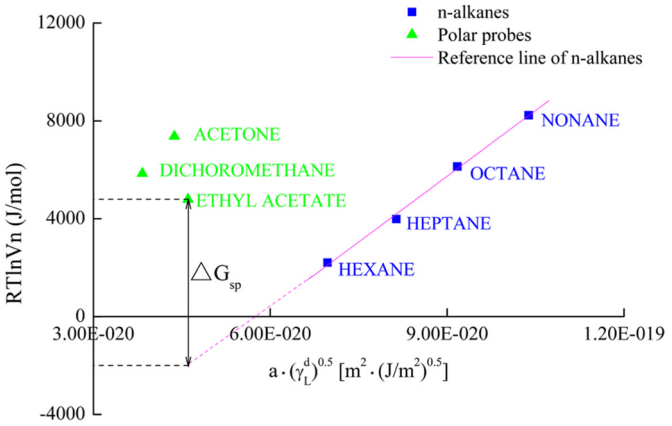

Fig. 2. Determination of dispersive surface energy and specific surface energy (lignite, $n/n_m = 0.3$).

where N_A is the number of Avogadro, $6.023 \times 10^{23}(mol^{-1})$; a is the cross sectional area of the probe (m^2); γ_s^d is the dispersive surface energy of the solid (mJ/m^2); γ_l^d is dispersive surface tension of the probe molecule in liquid state (mJ/m^2).

$$RT \ln V_N = 2V_N \gamma_s^d a \sqrt{\gamma_l^d} + \text{Constant} \quad (6)$$

To combine Eq. (4) and Eq. (5), a line equation $y = kx + b$ can be obtained, where $x = a\ (\gamma_l^d)^{0.5}$; $y = RT\ln V_N$, and γ_s^d can be determined from the slope.

Fig. 2 reports a typical determination of dispersive and specific surface energy at a certain surface converge ($n/n_m = 0.3$). If polar probes interact with the solid material, the ΔG has a contribution for the free specific interactions ΔG^{sp}.

Under different relative humidity circumstance, the existence forms of moisture will be different on the surface of the lignite particle and the surface energy will be different, as well. Fig. 3 displays the relationship between surface coverage and dispersive surface energy under the relative humidity 0% and 90%.

Fig. 3. shows the relationship between surface coverage n/n_m and dispersive surface energy of lignite (sample *f*). Under the coverage of $n/n_m = 0.01$, the addition of water had little influence on the dispersive energy. With the increase of coverage, both of the dispersive energy of wet and dry particles decrease. The surface energy of the sample with RH = 90% had larger dispersive energy. With the increase of surface energy coverage, the difference dispersive surface energy between the

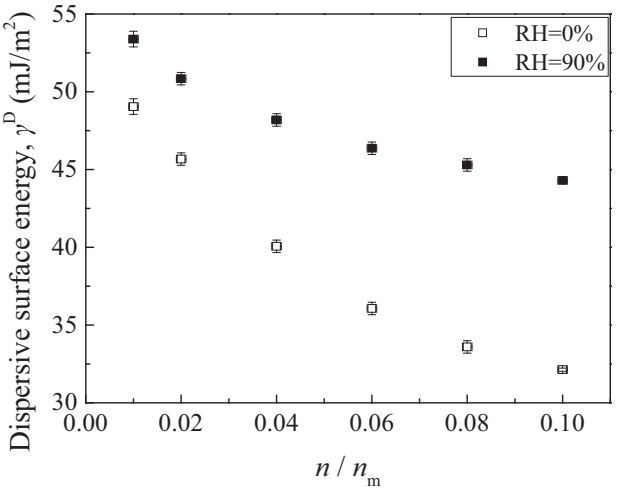

Fig. 3. The relationship between surface coverage n/n_m and dispersive surface energy of lignite (sample *f*).

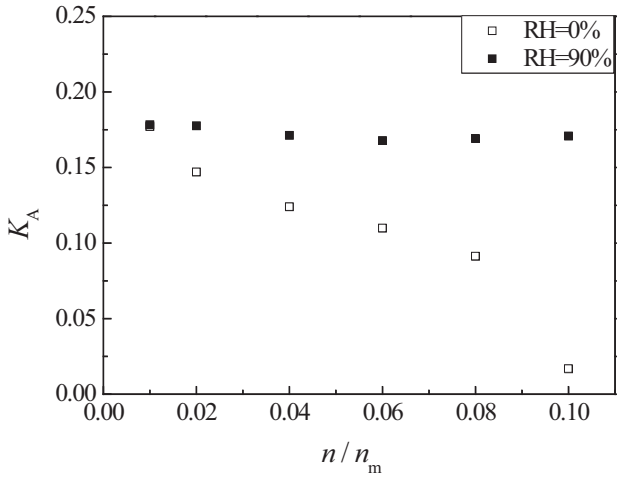

Fig. 4. Acid constant profiles (as a function of surface coverage n/n_m).

adsorbed and unadsorbed moisture lignite particle became larger. When the lignite particle adsorbed water, the dispersive energy became higher.

3.1.2. Acid base surface characteristic

The surface chemistry of the samples can be assessed with the Gutmann acid (K_A) and base (K_D) numbers. These numbers were related to the specific free energy of adsorption ($\triangle G^{SP}$) obtained with polar probe molecules [41–43] by means of the following relationship:

$$\Delta G^{sp} = K_D \cdot AN + K_A \cdot DN \quad (7)$$

where K_A and K_D are expressions of acidity and basicity of the surface layer of the tested material. *DN* is the donor number of the polar test compound, *AN* is the modified acceptor number. The Eq. (7) was divided by *AN*:

$$\frac{\Delta G^{sp}}{AN} = K_D + K_A \cdot \frac{DN}{AN} \quad (8)$$

And therefore K_A and K_D parameters were determined from the slope and intercept in a diagram in which the value of $\Delta G^{sp}/AN$ are plotted versus DN/AN for the different probe molecules.

The surface character of the examined material is characterized by the relative importance of K_A and K_D. $K_A > K_D$ indicates acidic character of the surface, and $K_A < K_D$ is typical of basic materials, while K_A value close to K_D value are typical for amphoteric materials. Fig. 4 and Fig. 5 showed the relationship between K_A (K_D) and surface coverage. When the lignite particle adsorbed moisture, the acid properties were enhanced. With the increase of surface coverage, the acid properties increased while the base properties remained nearly constant. For the lignite particle adsorbing moisture, the acid and base properties would not change with the increase of surface coverage, which meant that the polarity of the surface was turned to be uniform.

The acid and base surface properties of the tested materials are described by the value of K_A/K_D. When the value of K_A/K_D is higher than 1, the acid property is domain. On the contrary, the value of K_A/K_D is lower than 1, the base property is domain. If the value of K_A/K_D is equal to 1, the material has amphoteric material. What's more, the sum of $K_A + K_D$ describes the total polarity of the particle surface. Fig. 6 displays the particle surface is base. For the dry lignite particle, with the increase of surface coverage, the base properties of lignite particle are gradually enhanced. After adsorbing moisture, the base and acid properties of particle surface have no significant change under the low surface coverage. However, under the high surface coverage, the influence of acid property remained constant for the particles with RH = 90% and the influence of base property on the dry particle

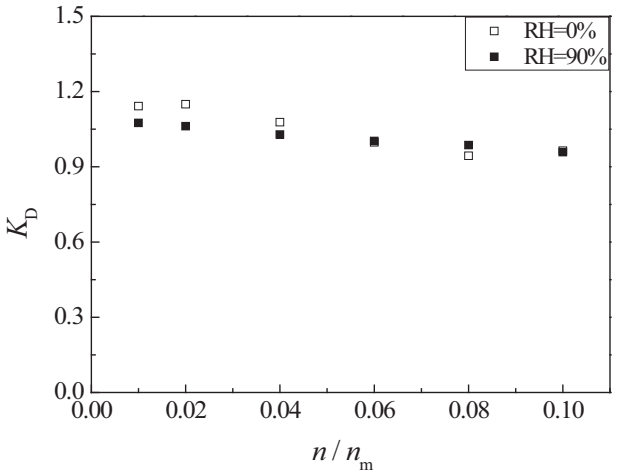

Fig. 5. Base constant profiles (as a function of surface coverage n/n_m).

became bigger. Although the acid and base properties have significant change, the total polarity of the lignite particle surface has no obvious change. With the increase of surface coverage, the sum of ($K_A + K_D$) decreased.

A better representation of the surface energy of materials can be provided by a surface energetic distribution (heterogeneity), as the solid surface is often heterogeneous and a single value for surface energy does not represent the whole surface. The SEA technique is able to provide also the surface energy heterogeneity of complex particulate solids. At low concentration of probe molecules, only high energy surface points are probed. As the coverage is increased, lower energy surfaces are probed. The total surface energy distribution and profiles was shown in Fig. 7. Under low surface coverage, moisture content will not influence the surface energy of the lignite particle. However, with the increase of surface coverage, the surface energy of RH = 90% was obviously higher than dry particle, which was contributed by the acid properties. After adsorbing the moisture, the distribution of surface energy became uniform. Because, the adsorbed moisture covered the roughness of particle surface, making the rough surface smoother and the surface properties more uniform. Through the surface energy test, under low surface coverage, the probe interacted with the high surface energy part, which contributed to the most surface energy. The surface energy test showed that the moisture didn't cover the particle. When the moisture is the form of interior moisture, there is no liquid bridge.

3.2. Bulk properties

Compressibility of the fuel powders were measured using the FT4 compression cell. The compressibility results were presented in Fig. 8. The relationship proposed by Tomas [44–46] was used to describe the compressibility of fuel powders:

$$\frac{\rho_b}{\rho_{b,0}} = \left[\frac{\sigma_1 + \sigma_{1,z}}{\sigma_{1,Z}}\right]^N \tag{9}$$

where $\rho_{b,0}$ is the powder bulk density under negligible consolidation, and $\sigma_{1,z}$ is the applied pull-off stress when the unconfined yield strength is zero. The parameter N is the compressibility index, in the range of 0–1. In particular, $N = 0$ indicates incompressibility and stiff bulk material, while $N = 1$ represents the compressibility of an ideal gas.

Fig. 8 gives the relationship between bulk density and particle sizes under different relative humidity. Fig. 9 gives the compressibility index. With the increase of particle size, the bulk density remains constant. The bulk density of wet samples is higher than the dry ones. But the compressibility of the different moisture content has no significant difference. In other words, the interior water will not influence the packing state of the particle. The increase of packing density with the water addition means that the adsorbed moisture existed in the pores of particles, making the gravity of particle higher. So, the packing test and surface energy test have common in that the adsorbed moisture in the materials are interior water.

3.3. Shear properties

The tensile strength is an indirect result of the shear tests, which can be obtained from the powder angle of internal friction and the powder cohesion. The tested pulverized coal under different moisture contents are assumed as the ideal Coulomb elastic–plastic powders. The powder yield followed the equation of Mohr-Coulomb. The dry and wet sample with different particle size distributions were tested by the FT4 shear test module.

Flow parameters are necessary to derive the unconfined yield strength σ_c, which is simply found from the linear yield locus [47]. The unconfined yield strength has the linear relationship with major principle stress [44]. The linear relationship between uniaxial tensile strength and major principal stress is like the relationship between unconfined yield strength and major principal stress. Fig. 10 showed that the linear relationship between tensile stress and major principal stress, which could be described by [44]:

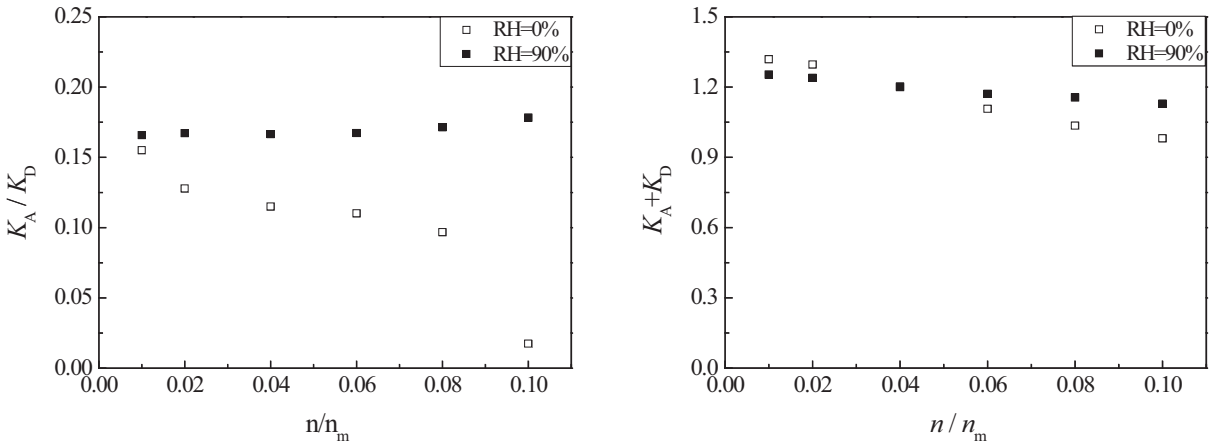

Fig. 6. Acid and base constant profiles (as a function of surface coverage n/n_m): (a) K_A/K_D; (b) $K_A + K_D$.

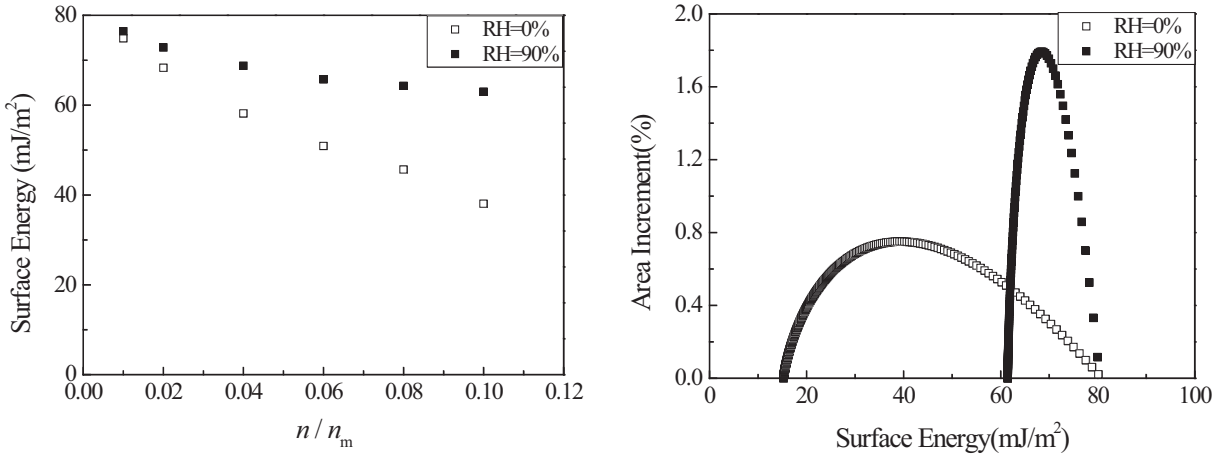

(a) (b)

Fig. 7. (a) Surface energy profiles (as a function of surface coverage n/n_m); (b) surface energy distribution.

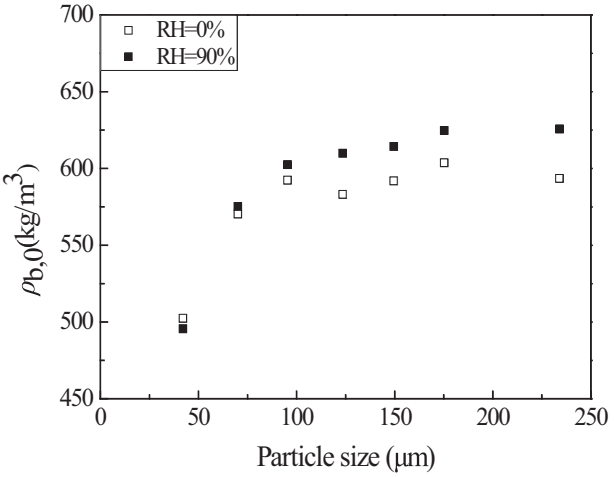

Fig. 8. Bulk density as function of particles size.

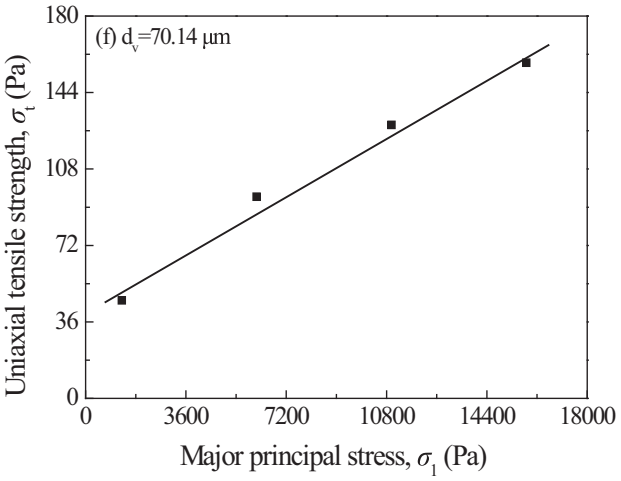

Fig. 10. Relationship between tensile stress and major principal stress.

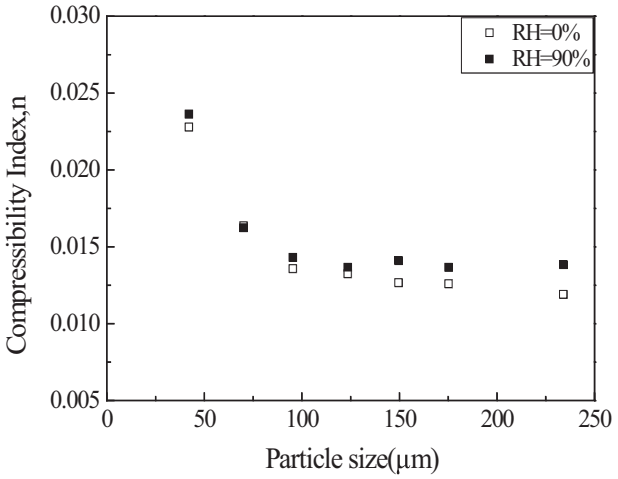

Fig. 9. Compressibility index as a function of particle size.

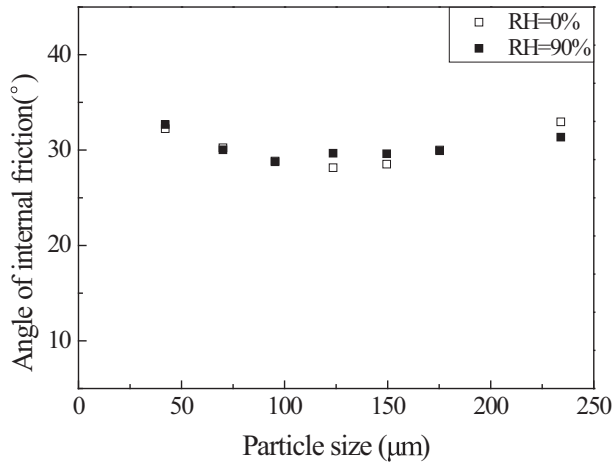

Fig. 11. Relationship between angle of internal friction and particle size.

$$\sigma_t = a_0\sigma_1 + \sigma_{z,0} = \frac{2(\sin\varphi_{st} - \sin\varphi_i)}{(1+\sin\varphi_{st})(1+\sin\varphi_i)}\sigma_1 + \frac{2\sin\varphi_{st}}{1+\sin\varphi_{st}}\sigma_0 \quad (10)$$

where the φ_{st} is the static angle of internal friction and σ_0 is the tensile strength under unconsolidated stress. Obviously, the flow behavior is mainly influenced by the difference between the friction angles ($\sin\varphi_{st}$-$\sin\varphi_i$).

Fig. 11 shows the relationship between angle of internal friction and

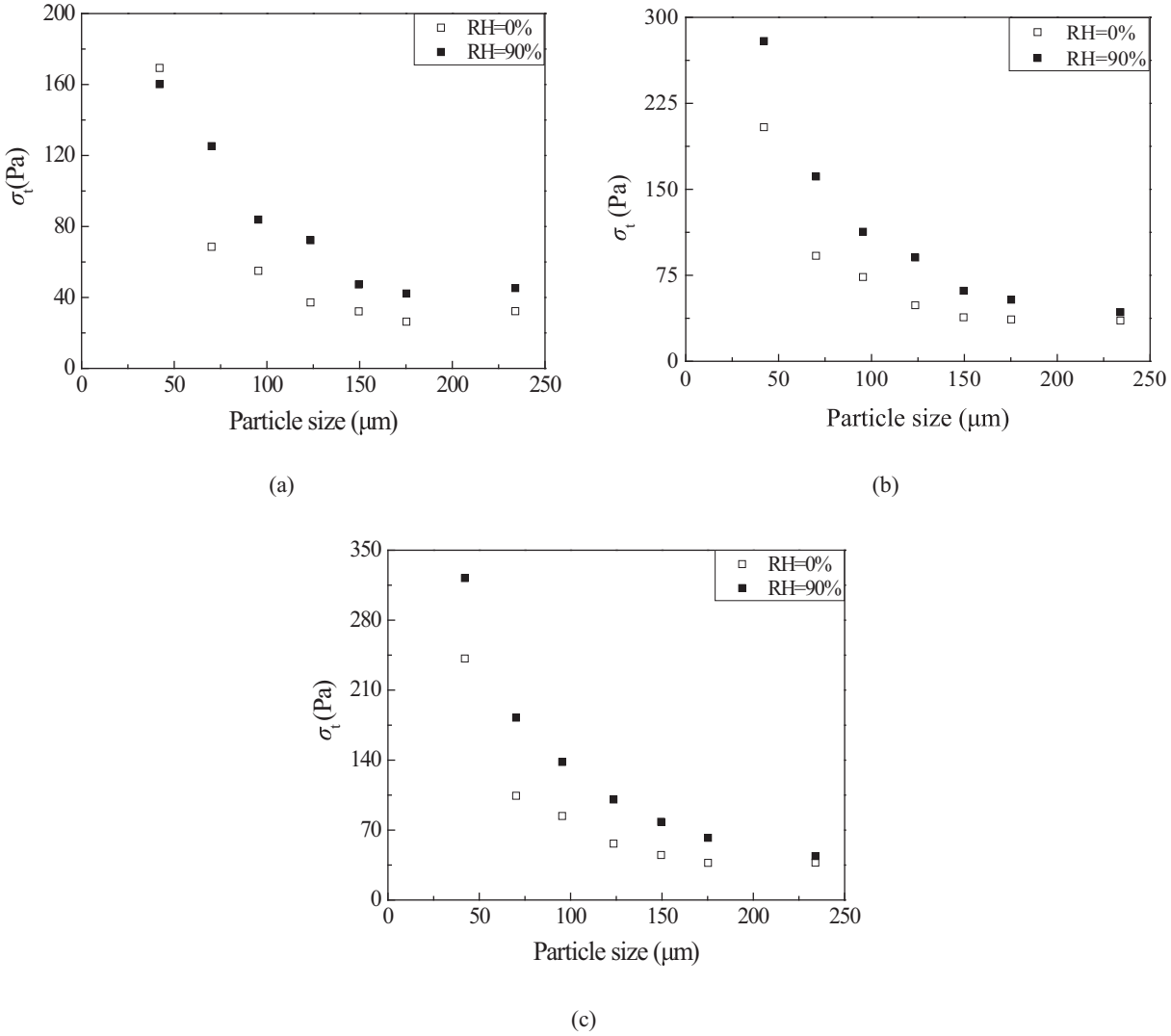

Fig. 12. Relationship between tensile strength and particle size under different preconsolidation: (a) 3 kPa, (b) 6 kPa, (c) 9 kPa.

particle size under different relative humidity. It is obvious that the adsorbed moisture doesn't influence the angle of internal friction greatly. Fig. 12 gives that the trend of the change of tensile strength. With the increase of particle size, the tensile strength decreases. For the larger particle, the addition of moisture has little influence on it. But for the small particle under the low consolidation stress, the addition of moisture will decrease the tensile strength. And for small particle, to some extent, the addition of moisture will improve the flowability.

3.4. Angle of repose

The angle of repose test shows the flowability of the particle when it is in a loose state. If the angle of repose is bigger, the flowability of the particle will become poorer.

Fig. 13 demonstrates the relationship between particle size and angle of repose under different moisture, which has the same trend with the relationship between tensile strength and particle size. When the particle size is larger than 150 μm, the value change of angle of repose is small. When the particle size is smaller than 150 μm, the value of angle of repose increases with the decrease of particle size. Meanwhile, the angle of repose of the material adsorbing the moisture is smaller than the dry one, indicating that the flowability was improved. Because for the large lignite coal particle (> 150 μm), the gravity force is higher than inter-particle force, like capillary force and van der Waals force. The influence of water addition increased the capillary force and van der Waals force. But they are still smaller than the gravity force [6]. Although the addition of moisture can make the gravity of the particle

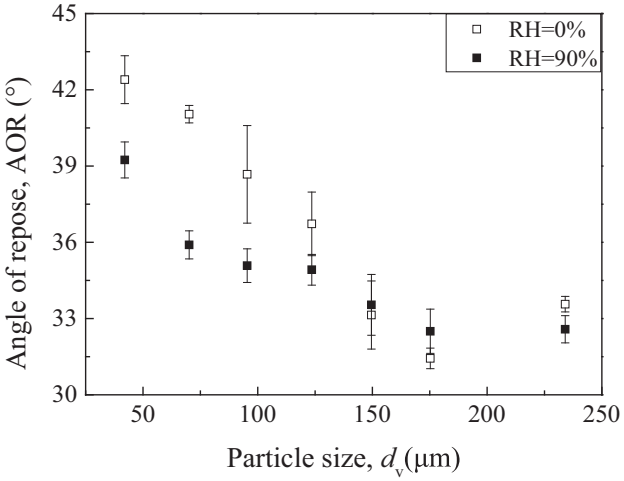

Fig. 13. Relationship between different particle size and angle of repose under different relative humidity.

larger, the change is not very obvious. However, for the small particle, the increase of gravity will improve the flowability. The moisture content is almost the same (seen in STbale1), the influence of water addition on flowability is small and the result of angle of repose is close. It means that the addition of moisture content will decrease the angle of repose and improve the powder flowability.

3.5. Model analysis

The angles of repose of the lignite particle are almost independent of the particle size for large particle size (> 150 μm). For smaller particle size, it steadily increases with the decrease of particle size. We all know that the differences between the bulk scale of the powder flow properties and the microscopic particle force, which could be described by surface energy as well as particle size, surface area, aggregation state etc. In order to describe the relationship between the flow properties and particle properties, a model is proposed.

It is a matter of common observation that the top surface of a mass of granular material can't be horizontal unlike that of a stagnant liquid. The angle of repose is defined as the angle of inclination of the free surface to the horizontal of a bulk solid pile when it is in a state of maximum static. There is an upper limit to the slope of the top surface and the angle between this maximum slope and the horizontal, which is known as the angle of repose. If there is a planar slope inclined at the angle θ to the horizontal. (Seen in Fig. 14) For a cohesive material there is a relationship between the angle of repose and the heap height [48]. The greatest value of θ for stability is given by $\theta = \varphi_i$. So the angle of repose equals the angle of internal friction φ_i. The angle of repose is defined as the angle of inclination of the free surface to the horizontal of a bulk solid pile when it is in a state of maximum static, which is independent of the extent of the inclined surface. The height is proportional to the tangent of angle of repose, $\tan\theta = k\,h$. The maximum height of a vertical slope is given by [48]:

$$h = \frac{4C\cos\varphi_i}{\rho_{b,0}g(1-\sin\varphi_i)} \tag{11}$$

where C is cohesive strength, $\rho_{b,0}$ is the bulk density at negligible consolidation, g is the gravitational acceleration, with φ_i values of the effective angle of internal friction assumed to be around 30°, according to the experiment results. Thus, Eq. (11) could be changed into:

$$h = \frac{4\sqrt{3}C}{\rho_{b,0}g} \tag{12}$$

The cohesive strength C is proportional to the inter-particle force F_{ad} and the number of inter-particle contacts per unit fracture area n_c, one obtained:

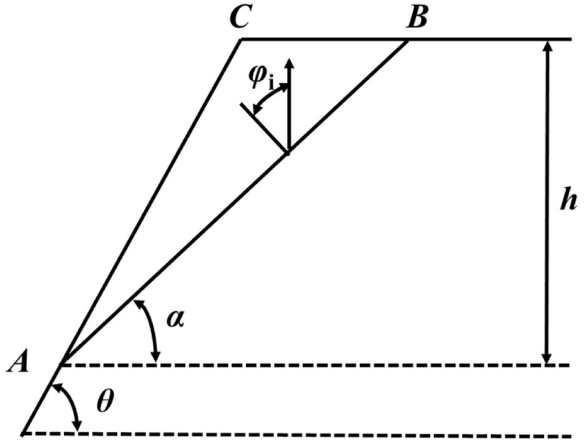

Fig. 14. Slip plane for the failure of a slope.

$$C = k_1 \cdot n_c \cdot F_{ad} \tag{13}$$

where, the real number of contacts per unit fracture surface area, n_c, is the combination of the number of macroscopic interparticle contacts per unit fracture surface area, n_{pp} and number of micro-contacts n_{cp} and $n_c = k_2\, d_s \varphi^m/(1\text{-}\varphi)$ [49]. In this paper, van der Waals force is the main inter-particle force, F_{ad}, which was positive correlation with particle size and surface energy of the particles. The inter-particle force F_{ad} may be expressed as:

$$F_{ad} = k_3 d_s \cdot \gamma \tag{14}$$

where is d_s mean surface diameter of the particles, m; γ is surface energy, mJ/m^2. φ is the bed compactness, which assumed to be $\rho_{b,0}/\rho_p$ in this study. The Eq. (14) and Eq. (13) were taken into the Eq. (12) and according to the assumption, the vertical height was proportional to the tangent of angle of repose. So the angle of repose could be expressed as:

$$\tan AOR = k_4 \frac{\gamma}{\rho_{b,0}g} \cdot \frac{\varphi^m}{1-\varphi} d_s^{-p} \tag{15}$$

Finally, the expression of angle of repose will be simplified as:

$$\tan AOR = K \frac{\varphi^m}{1-\varphi} d_s^{-p} \tag{16}$$

where K is related to materials' density and surface energy, $K = k_4\gamma/(\rho_{b,0}g)$ and parameters m and p related to the surface topography of particles, including surface roughness, particle shape etc., which could be obtained from the regression with the experiment data. The bed compactness, φ, has already been obtained according to the compressibility test results section. According to the Eq. (16), the angle of repose was related to the particle surface energy, bulk and flow properties.

Fig. 15 and Fig. 16 show the angle repose comparison of model value and experiment data. The deviation between model and experiment is within ± 2%. Model parameter is showed in Table 3. Model parameter K stands for the particle properties term, including surface energy and bulk density. With the increase of relative humidity, the surface energy increases and the bulk density increases, as well. But the gradient is different. The increase of bulk density is higher than the one of surface energy. In other words, with the increase of moisture content, the bulk density plays a more important role. And the surface energy of the particle becomes less important, which is the same as before. The parameter p stands for the influence of particle size. The values are positive, but they give to the negative contributions. If the particle size increases, the angle of repose decreases. This is the same to the experiment value.

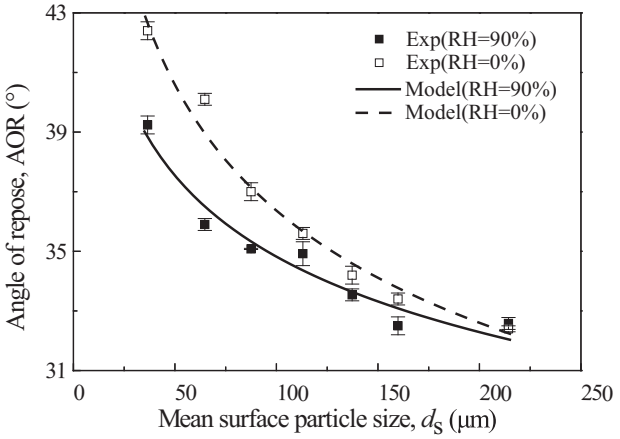

Fig. 15. Comparison of the model calculation and experimental data for the angle of repose.

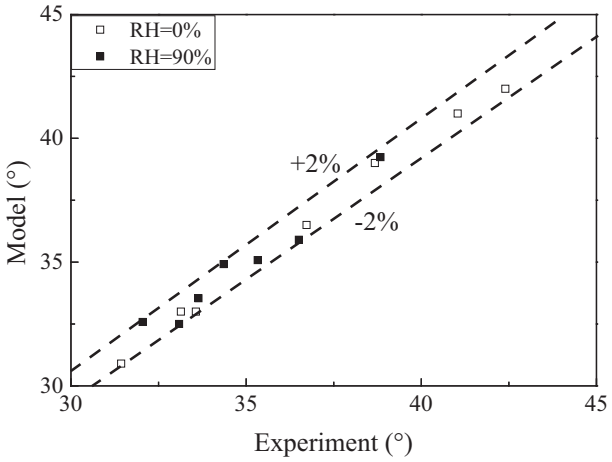

Fig. 16. Comparison of model and experiment value of angle of repose.

Table 3
Model parameters (K, m, p) under different relative humidity.

	K	m	p
RH = 0%	0.6713	1.095	0.1762
RH = 90%	0.4243	0.9667	0.1115

4. Conclusions

Through the surface energy test, bulk and shear properties test, the seven different particle size distribution lignite particle samples under relative humidity of 90% and 0% were analyzed.

1. The surface energy test indicates that the moisture in the particle was interior water, which existed in the pores and not on the surface of the particle. The particle adsorbing the moisture content would make the surface of the particle more uniform.
2. The compressibility test shows that the increase of moisture content will influence the bulk density. But it has no obvious effect.
3. Through the shear test, the angle of internal friction results show that the interior water doesn't influence internal friction of lignite. To some extent, this kind of moisture will improve the flowability of lignite.
4. In the end, the model involving in the surface energy and flowability was proposed to predict the angle of repose of the dry and wet lignite particles with different particle size distribution. The model analysis showed agreement with the experiment and the modelling error was between −2% and + 2%.

Acknowledgements

This work was supported by the National Natural Science Foundation of China (21206041), and Shanghai Science and Technology Commission Project (14DZ1200100, 15DZ1200802), the Fundamental Research Funds for the Central Universities (222201717004, 222201514338) and the Key Scientific Research Project in Shanxi (MH2014-01).

Appendix A. Supplementary data

Supplementary data to this article can be found online at https://doi.org/10.1016/j.fuproc.2018.02.024.

References

[1] Z. Dai, X. Gong, X. Guo, H. Liu, F. Wang, Z. Yu, Pilot-trial and modeling of a new type of pressurized entrained-flow pulverized coal gasification technology, Fuel 87 (2008) 2304–2313.
[2] X. Guo, Z. Dai, X. Gong, X. Chen, H. Liu, F. Wang, Z. Yu, Performance of an entrained-flow gasification technology of pulverized coal in pilot-scale plant, Fuel Process. Technol. 88 (2007) 451–459.
[3] A.J. Minchener, Coal gasification for advanced power generation, Fuel 84 (2005) 2222–2235.
[4] Q. Zhuang, M. Biondi, S. Yan, K. Bhagat, R. Vansickle, C. Chen, H. Tan, Y. Zhu, W. You, W. Xia, TRIG™: an advanced gasification technology to utilize low rank coals for power, Fuel 152 (2015) 103–109.
[5] C.-Z. Li, Importance of volatile–char interactions during the pyrolysis and gasification of low-rank fuels – a review, Fuel 112 (2013) 609–623.
[6] Y. Jin, H. Lu, X. Guo, X. Gong, Effect of water addition on flow properties of lignite particles, Chem. Eng. Res. Des. 132C (2018) 1020–1029.
[7] H. Lu, X. Guo, Y. Jin, X. Gong, Dense-feeding of pulverized coal into the entrained-flow gasifier, Ind. Eng. Chem. Res. 56 (2017) 9734–9742.
[8] X. Fu, D. Huck, L. Makein, B. Armstrong, U. Willen, T. Freeman, Effect of particle shape and size on flow properties of lactose powders, Particuology 10 (2012) 203–208.
[9] J.J. Fitzpatrick, S.A. Barringer, T. Iqbal, Flow property measurement of food powders and sensitivity of Jenike's hopper design methodology to the measured values, J. Food Eng. 61 (2004) 399–405.
[10] G. Bruni, P. Lettieri, D. Newton, J. Yates, The influence of fines size distribution on the behaviour of gas fluidized beds at high temperature, Powder Technol. 163 (2006) 88–97.
[11] Y. Liu, X. Guo, H. Lu, X. Gong, An investigation of the effect of particle size on the flow behavior of pulverized coal, Powder Technol. 284 (2015) 47–56.
[12] Y. Liu, H. Lu, X. Guo, X. Gong, X. Sun, Z. Zhang, The influence of fine particles on bulk and flow behavior of pulverized coal, Powder Technol. 303 (2016) 212–227.
[13] Y. Liu, H. Lu, M. Poletto, X. Guo, X. Gong, Bulk flow properties of pulverized coal systems and the relationship between inter-particle forces and particle contacts, Powder Technol. 322 (2017) 226–240.
[14] R. Ho, S.E. Dilworth, D.R. Williams, J.Y.Y. Heng, Role of surface chemistry and energetics in high shear wet granulation, Ind. Eng. Chem. Res. 50 (2011) 9642–9649.
[15] F. Fichtner, D. Mahlin, K. Welch, S. Gaisford, G. Alderborn, Effect of surface energy on powder compactibility, Pharm. Res. 25 (2008) 2750–2759.
[16] V. Karde, C. Ghoroi, Fine powder flow under humid environmental conditions from the perspective of surface energy, Int. J. Pharm. 485 (2015) 192–201.
[17] J.F. Gamble, R.N. Davé, S. Kiang, M.M. Leane, M. Tobyn, S.S. Wang, Investigating the applicability of inverse gas chromatography to binary powdered systems: an application of surface heterogeneity profiles to understanding preferential probe-surface interactions, Int. J. Pharm. 445 (2013) 39–46.
[18] L. Lapcik, B. Lapcikova, E. Otyepkova, M. Otyepka, J. Vlcek, F. Bunka, R.N. Salek, Surface energy analysis (SEA) and rheology of powder milk dairy products, Food Chem. 174 (2015) 25–30.
[19] C. Sun, J.C. Berg, The effective surface energy of heterogeneous solids measured by inverse gas chromatography at infinite dilution, J. Colloid Interface Sci. 260 (2003) 443–448.
[20] J.F. Gamble, M. Leane, D. Olusanmi, M. Tobyn, E. Supuk, J. Khoo, M. Naderi, Surface energy analysis as a tool to probe the surface energy characteristics of micronized materials–a comparison with inverse gas chromatography, Int. J. Pharm. 422 (2012) 238–244.
[21] R. Rajkhowa, A. Kafi, Q.T. Zhou, A. Kondor, D.A.V. Morton, X. Wang, Relationship between processing, surface energy and bulk properties of ultrafine silk particles, Powder Technol. 270 (2015) 112–120.
[22] K.S. Chang, D.W. Kim, S.S. Kim, M.Y. Jung, Bulk flow properties of model food powder at different water activity, Int. J. Food Prop. 1 (1998) 45–55.
[23] R. Li, Y.H. Roos, S. Miao, The effect of water plasticization and lactose content on flow properties of dairy model solids, J. Food Eng. 170 (2016) 50–57.
[24] P. Shenoy, E. Xanthakis, F. Innings, C. Jonsson, J. Fitzpatrick, L. Ahrné, Dry mixing of food powders: effect of water content and composition on mixture quality of binary mixtures, J. Food Eng. 149 (2015) 229–236.
[25] Y. Tu, Z. Xu, W. Wang, Method for evaluating packing condition of particles in coal water slurry, Powder Technol. 281 (2015) 121–128.
[26] E.C. Abdullah, D. Geldart, The use of bulk density measurements as flowability indicators, Powder Technol. 102 (1999) 151–165.
[27] E. Emery, J. Oliver, T. Pugsley, J. Sharma, J. Zhou, Flowability of moist pharmaceutical powders, Powder Technol. 189 (2009) 409–415.
[28] F. Fichtner, D. Mahlin, K. Welch, S. Gaisford, G. Alderborn, Effect of surface energy on powder compactibility, Pharm. Res. 25 (2008) 2750–2759.
[29] K.L. Johnson, K. Kendall, A.D. Roberts, Surface energy and the contact of elastic solids, Proceedings of the Royal Society A, 324 1971, pp. 301–313.
[30] V. Karde, C. Ghoroi, Influence of surface modification on wettability and surface energy, Int. J. Pharm. 475 (2014) 351–363.
[31] L. Lapčík, E. Otyepková, B. Lapčíková, M. Otyepka, Surface energy analysis (SEA) study of hyaluronan powders, Colloids Surf. A Physicochem. Eng. Asp. 436 (2013) 1170–1174.
[32] D. Macrì, D. Barletta, P. Lettieri, M. Poletto, Experimental and theoretical analysis of TiO2 powders flow properties at ambient and high temperatures, Chem. Eng. Sci. 167 (2017) 172–190.
[33] R. Chirone, D. Barletta, P. Lettieri, M. Poletto, Bulk flow properties of sieved samples of a ceramic powder at ambient and high temperature, Powder Technol. 288 (2016) 379–387.
[34] I. Tomasetta, D. Barletta, M. Poletto, Correlation of powder flow properties to interparticle interactions at ambient and high temperatures, Particuology 12 (2014)

90–99.
[35] G. Landi, D. Barletta, M. Poletto, Modelling and experiments on the effect of air humidity on the flow properties of glass powders, Powder Technol. 207 (2011) 437–443.
[36] E. Teunou, J.J. Fitzpatrick, Effect of relative humidity and temperature on food powder flowability, J. Food Eng. 42 (1999) 109–116.
[37] A.M. Goula, K.G. Adamopoulos, Effect of maltodextrin addition during spray drying of tomato pulp in dehumidified air: II. Powder properties, Dry. Technol. 26 (2008) 726–737.
[38] G. Landi, D. Barletta, P. Lettieri, M. Poletto, Flow properties of moisturized powders in a couette fluidized bed rheometer, Int. J. Chem. React. Eng. 10 (1) (2012) 1205–1224.
[39] R.P. Dugar, R.H. Dave, The effects of solvent and relative humidity on rheological and thermal properties of microcrystalline cellulose granules using hydroxypropyl methylcellulose as binder, Int. J. Pharm. Sci. Res. 5 (2014) 3616–3626.
[40] F.L.J. Riddle, F.M. Fowkes, Spectral shifts in acid-base chemistry. Part 1. van der Waals contributions to acceptor numbers, J. Am. Chem. Soc. 112 (1990) 3259–3264.
[41] J. Schultz, L. Lavielle, C. Martin, The role of the interface in carbon fibre-epoxy composites, J. Adhes. 23 (1987) 45–60.
[42] M. Przybyszewska, A. Krzywania, M. Zaborski, M.I. Szynkowska, Surface properties of zinc oxide nanoparticles studied by inverse gas chromatography, J. Chromatogr. A 1216 (2009) 5284–5291.
[43] B. Strzemiecka, J. Kołodziejek, M. Kasperkowiak, A. Voelkel, Influence of relative humidity on the properties of examined materials by means of inverse gas chromatography, J. Chromatogr. A 1271 (2013) 201–206.
[44] J. Tomas, Fundamentals of cohesive powder consolidation and flow, Granul. Matter 6 (2004) 75–86.
[45] M. Mohan, B. Pitchumani, J. Tomas, Flow characterization of fine powders using material characteristic parameters, Adv. Powder Technol. 16 (2005) 123–135.
[46] J. Thomas, Product design of cohesive powders–mechanical properties, compression and flow behavior, Chem. Eng. Technol. 27 (2010) 605–618.
[47] J. Tomas, Product design of cohesive powders – mechanical properties, compression and flow behavior, Chem. Eng. Technol. 27 (2004) 605–618.
[48] R.M. Nedderman, Statics and Kinematics of Granular Materials, Cambridge University Press, 1992.
[49] C.H.H. Rumpf, Zur Theorie der Zugfestigkeit von Agglomeraten bei Kraftübertragung an Kontaktpunkten, Chemie Ingenieur Technik 42 (1970) 538–540.